Environmental Modelling and Software 134 (2020) 104884

Contents lists available at ScienceDirect

Environmental Modelling and Software

journal homepage: http://www.elsevier.com/locate/envsoft

Spatially explicit reconstruction of post-megafire forest recovery through landscape modeling

Wenru Xu[a], Hong S. He[a,*], Jacob S. Fraser[b], Todd J. Hawbaker[c], Paul D. Henne[c], Shengwu Duan[a], Zhiliang Zhu[d]

[a] School of Natural Resources, University of Missouri, 203 ABNR Bldg., Columbia, MO, 65211, USA
[b] USDA Forest Service, Northern Research Station, 202 ABNR Bldg., Columbia, MO, 65211, USA
[c] U.S. Geological Survey, Denver Federal Center, MS 980, Denver, CO, 80225, USA
[d] U.S. Geological Survey, 12201 Sunrise Valley Drive, Reston, VA, 20192, USA

ARTICLE INFO

Keywords:
Megafire
Reconstruction
Forest landscape model
Remote sensing
Field inventory

ABSTRACT

Megafires are large wildfires that occur under extreme weather conditions and produce mixed burn severities across diverse environmental gradients. Assessing megafire effects requires data covering large spatiotemporal extents, which are difficult to collect from field inventories. Remote sensing provides an alternative but is limited in revealing post-fire recovery trajectories and the underlying processes that drive the recovery. We developed a novel framework to spatially reconstruct the post-fire time-series of forest conditions after the 1987 Black Dragon fire of China by integrating a forest landscape model (LANDIS) with remote sensing and inventory data. We derived pre-fire (1985) forest composition and the megafire perimeter and severity using remote sensing and inventory data. We simulated the megafire and the post-megafire forest recovery from 1985 to 2015 using the LANDIS model. We demonstrated that the framework was effective in reconstructing the post-fire stand dynamics and that it is applicable to other types of disturbances.

1. Introduction

Forest fire is a primary disturbance in many forest ecosystems, influencing succession dynamics and carbon storage (Lecomte et al., 2006; Bowman et al., 2009). Fires that burned large areas with high intensity (areal extent > 100 km^2, often called megafires) can cause abrupt changes to ecosystems and have distinctly different ecological effects from other fires (Bradstock, 2008; Keane et al., 2008; Stephens et al., 2014). Post-fire recovery is an important variable for understanding fire effects on forest ecosystems, which is mainly determined by burn severity and species regeneration strategies (Johnstone et al., 2010; Halofsky et al., 2011). Megafires often result in a heterogeneous mosaic of burn severities across a wide range of environmental conditions; consequently, the vegetational response can be complex. Seedlings regenerated after the fire vary strongly among areas with contrasting burn severities due to species-specific differences in dispersal, seed size, shade tolerance and parent tree locations. Large-seeded species (e.g., *Pinus* spp.) have higher regeneration rates under partial shade, and thus have higher regeneration rates in areas with low or moderate severity burns, while fecund, light-seeded broadleaf species (e.g., *Betula* spp.) are wind dispersed and are more likely to colonize in areas with high severity burns (Greene et al., 2007; Johnstone et al., 2010). Megafires can also create large high-severity burn patches that could delay tree regeneration and prolong early seral conditions by limiting the reach of seed dispersal (Johnstone et al., 2016), which may even trigger a shift from forest to shrub- or grass-dominated cover types due to seed limitation and climate-induced regeneration failure (Collins and Roller, 2013; Savage et al., 2013; Harvey et al., 2016). Even with similar burn severity and sufficient seed availability, germination and establishment can be affected by tolerances to temperature and moisture that vary by species (Petrie et al., 2016; Davis et al., 2018) and microsite conditions, which can influence the success of tree establishment and regeneration, with fewer tree seedlings found on harsh sites (Broncano and Retana, 2004; Bonnet et al., 2005; Kemp et al., 2019). The complex vegetation responses to megafires make assessments of post-fire recovery challenging.

Assessment of post-fire forest recovery is traditionally completed with plot-based field inventories. This method can provide relatively

* Corresponding author.
E-mail address: heh@missouri.edu (H.S. He).

https://doi.org/10.1016/j.envsoft.2020.104884
Accepted 29 September 2020
Available online 6 October 2020

accurate and detailed measurements of post-fire plant communities, which can be used to quantify burn severity and recovery based on the time the plots were surveyed after the fire (e.g., Johnstone et al., 2004; Turner et al., 2016). However, field-based inventories generally cover small spatial extents and provide plot-based information on burn severity and recovery but not about the size and shape of burned patches (e.g., Crotteau et al., 2013). Since megafires burn large areas across a range of environmental gradients and a mix of burn severities, it is challenging to capture the heterogeneous burn severities and post-fire recovery patterns using field-based methods alone. In addition, forest inventories before and immediately after megafires, and the subsequent monitoring of vegetation recovery, are often lacking. These limitations hinder field-based approaches for assessing megafire effects and post-fire recovery.

Remote sensing is effective in capturing burn severity patterns and monitoring post-fire vegetation recovery for megafires (French et al., 2008; Gitas et al., 2012; Chu and Guo, 2014). Remote sensing-based vegetation indices such as the normalized burn ratio (NBR) (García and Caselles, 1991; Epting et al., 2005) and its derivatives, differenced NBR (dNBR) and relative differenced NBR (RdNBR) (Key and Benson, 2005; Miller and Thode, 2007), have been widely used for detecting burn severity patterns (Eidenshink et al., 2007). The normalized difference vegetation index (NDVI), enhanced vegetation index (EVI) and soil adjusted vegetation index (SAVI) have been used for monitoring post-fire recovery (van Leeuwen et al., 2010; Gitas et al., 2012; Veraverbeke et al., 2012). However, a great deal of uncertainty exists when using these vegetation indices to assess post-fire recovery in terms of species composition and forest structure. Forest recovery assessments using vegetation indices can become complicated when different vegetation recovery states have similar vegetation index values (Glenn et al., 2008; Chu and Guo, 2014). For instance, young (e.g., two years post-fire) broadleaf forest pixels may exhibit the same NDVI value as the unburned coniferous forest pixels that are on a very different successional stage (Idris et al., 2005; Cuevas-Gonzalez et al., 2009; Cai et al., 2018). The limited availability of cloud-free satellite images during the growing season can also impede continuous assessment of post-fire forest recovery (Ju and Roy, 2008). In addition, remote sensing-based vegetation indices are limited in their ability to monitor demographic processes such as seed dispersal, tree establishment and mortality, species competition, and competition-caused mortality (self-thinning), which drive post-fire forest recovery.

Fire-succession models have been used to understand the interactions between vegetation response to forest fire, including post-fire forest structure, composition, and diversity (Boychuk et al., 1997; Millington et al., 2009; Miller and Ager, 2013). However, most of these models lack demographic processes to capture the species regeneration traits. Alternatively, Forest landscape models (FLMs) spatially simulate forest dynamics (seed establishment, growth, competition, and succession) accounting for the processes not captured by remote sensing and fire-succession models, and have been effectively applied to spatially reconstructing historical post-disturbance forest conditions (He, 2008; Seidl et al., 2014; Thrippleton et al., 2014). FLMs can also incorporate information from fire perimeters and the spatial patterns of burn severity derived from remote sensing as inputs (Wang et al., 2009). They can track the location and abundance of parent trees and seedlings when simulating the demographic processes that drive post-fire forest recovery (Wang et al. 2013, 2014abib_Wang_et_al_2013bib_Wang_et_al_2014a). Finally, FLMs can be calibrated and validated with forest inventory data (Seidl et al., 2012; Wang et al., 2014b; Luo et al., 2015).

The 1987 Black Dragon fire, which occurred in the boreal forest of China, stood out due to its size and severity. The fire burned 1.3×10^4 km^2, resulted in a high degree of tree mortality, and reset forest succession for most burned stands. It created opportunities to study post-fire forest dynamics at an unprecedented scale. In this study, our objectives were to (1) present a novel framework that integrates an FLM with field inventory and remote sensing data to spatially reconstruct the burn severity of the Black Dragon fire and the post-fire time series of forest conditions (i.e., forest composition, structure and aboveground biomass) and (2) evaluate whether the reconstructed forest conditions could realistically capture the post-fire recovery (e.g., density and basal area) at the level of individual tree species under different burn severities. Spatiotemporal reconstruction of the post-megafire forest condition provides a platform to investigate the recovery rate and trajectories through model simulations and thus improve realism and reduce uncertainties.

2. Data and methods

2.1. Study area

Our study area is located in the Great Xing 'an Mountains and encompasses approximately 8.46×10^4 km^2 (50°10′ N, 121°12′ E to 53°33′ N, 127°00' E) in Northeast China. (Fig. 1). The area is hilly and mountainous (altitudes ranging from 134 to 1511 m) and falls within the continental cold temperate climate zone with long and severe winters but short summers. The average annual temperature is −3.9 °C with an average temperature of −33 °C in the coldest month (January), and an average temperature of 17.5 °C in the hottest month (July). The annual cumulative precipitation ranges from 400 to 500 mm. More than 60% of the annual precipitation occurs in the summer season from June to August (Zhou, 1991; Xu, 1998). Vegetation in this region is representative of cool boreal coniferous forests that cover 83% of the study area. The canopy species composition is relatively simple. Dahurian larch (*Larix gmelini* (Rupr.) Kuzen, hereafter "larch"), a deciduous conifer, and white birch (*Betula platyphylla* Suk.), a deciduous broadleaved species, are dominant, covering more than 80% of the study area. Other tree species include the evergreen conifers, Korean spruce (*Picea koriensis* Nakai, hereafter "spruce") and Scots pine (*Pinus sylvestris* var. *mongolica* Litvinov, hereafter "pine"), and the deciduous broadleaved species, aspen (*Populus davidiana* Dole and *P. suaveolens* Fischer), willow (*Chosenia arbutifolia* (Pall.) A. Skv), Asian black birch (*Betula davurica* Pall., hereafter "black birch"), and Mongolian oak (*Quercus mongolica* Fisch.ex Ledeb.). Black birch and Mongolian oak are mainly distributed in the southeastern low elevation part of the study area, whereas pine is distributed in the northern part.

Wildfire frequency and area burned in our study area are linked to

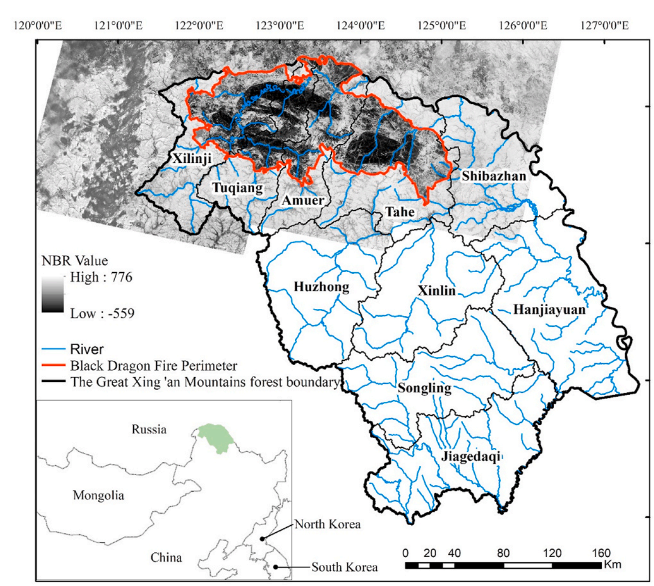

Fig. 1. The location of study area and the Black Dragon fire with Landsat 5 derived normalized burn ratio (NBR) values. The boundaries of the 10 forest bureaus are shown with thin black lines.

human disturbances and annual variations in monsoonal strength (Liu et al., 2012). Low intensity surface fires (mean return interval ca. 30 yr) were historically frequent, occasionally mixed with infrequent stand-replacing fires (mean return interval ca. 120 yr) in the high elevation regions (Xu et al., 1997). However, long-term fire exclusion and timber harvest have altered the fire regime, where fires are infrequent but more intense (Chang et al., 2007). In our study area, fires burned 6.64×10^4 km^2 from 1967 to 2005 (Chang et al., 2008; Liu et al., 2012). One of the most noteworthy fires, known as the Black Dragon fire, ignited on May 6, 1987 and burned four forest bureaus (Xilinji, Tuqiang, Amuer, and Tahe). The Black Dragon fire resulted in over 200 deaths and 4 billion Yuan of losses at that time, causing the most forest fire damage in the history of China.

2.2. General approach

We first reconstructed forest stand conditions in our study area before the Black Dragon fire (i.e., in 1985) using remote sensing and forest inventory data (Fig. 2). Since the remote sensing data could not provide detailed stand information at the pixel level across our entire landscape and pre-fire field inventory data were not available, we constructed the pre-fire forest conditions following the k-Nearest Neighbor (kNN) stand imputation approach of Zhang et al. (2018a, 2018b). We used Landsat data to delineate fire perimeters and derive burn severity classes associated with total tree mortalities (Xu et al., 2020). With the pre-fire landscape as a starting point, we 'burned in' the Black Dragon fire perimeter and severity in LANDIS PRO at the fire year 1987 and simulated the post-megafire time series forest conditions using a forest landscape model (LANDIS PRO) (Fig. 2).

LANDIS PRO has been parameterized for numerous forest regions under different environmental settings (Huang et al., 2018; Wang et al., 2019). However, to ensure tree species parameters of the model (e.g., growth rate, available seeds, maximum stand density index, and maximum diameter) accurately captured the tree species in our study area, we used a data assimilation approach (Luo et al., 2011; Wang et al., 2014b) that iteratively calibrated the parameters by comparing the simulated results at years with the respective forest inventory data (Fig. 2a). The calibration process was followed by validation against field inventory data at a later stage (2015) to ensure that forest dynamics under no disturbance were correctly simulated (Fig. 2a). To ensure the

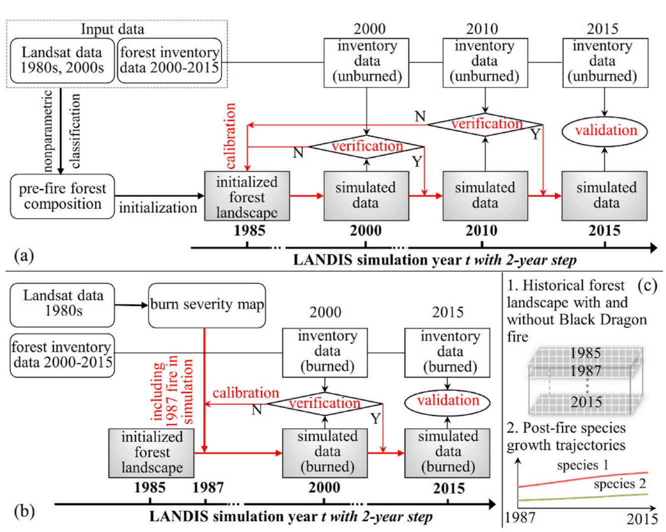

Fig. 2. The framework of reconstructing historical forest conditions and post-megafire recovery trajectories of density and basal area at species level. (a) Calibrating tree species parameters to constrain tree species growth strategies. (b) Calibrating fire parameters to constrain fire-caused mortality. (c) The outcome of the calibration and validation processes is the time-series post-fire forest conditions at species level.

response of tree species corresponded to various burn severities, we also applied the data assimilation approach to calibrate fire parameters (e.g., height of bark charring) in LANDIS PRO to precisely constrain post-fire tree species recovery processes (Fig. 2b). We used the year 2000 post-fire inventory data for the calibration and used the year 2015 post-fire inventory data for model validation since these were the only post-fire inventory data available in the burned area (Fig. 2b). Through the iterative calibration and validation processes, we were able to derive the continuous time-series forest conditions from which post-fire forest landscape recovery could be analyzed spatially and temporally (Fig. 2c).

2.3. Forest inventory data

The forest inventory data used for model initialization, calibration, and results validation in this study were collected from the China Forestry Science Data Center (CFSDC, http://www.cfsdc.org), including forest plot inventory data from 2000, 2010, and 2015, and a forest stand map in polygons with relatively complete attributes from the early 2000s (Fig. S1). The plot inventory data includes 5752 unburned plots and 1305 burned plots following the Black Dragon fire. Each plot contained the number of trees and diameter at breast height (DBH >5 cm) class by species. The forest stand map comprised 276,273 stands with homogeneous forest attributes (e.g., dominant tree species, stand age, and site index) in each stand. The data contained stand area, mean DBH, stand height, stand age, stand volume, tree species composition (species percent volume), forest origin (natural regeneration vs. afforestation), and management and disturbances (harvest, plantation and forest fires) information in each stand polygon.

2.4. Remote sensing data

In this study, 20 pre- and post-fire Landsat TM (Thematic Mapper) images (Table S1) from the U.S. Geological Survey (USGS, http://earthexplorer.usgs.gov) were used to estimate pre-fire forest composition and burn severity of the 1987 Black Dragon fire. The images were processed by the USGS to convert from DN (digital numbers) to surface reflectance using the LEDAPS algorithm (Landsat Ecosystem Disturbance Adaptive Processing System, Masek et al., 2006). Clouds, cloud shadows, and snow pixels were masked using the function of mask algorithm (FMASK; Zhu and Woodcock, 2012). The 1980s images were processed by radiometric normalization based on the images from the 2000s, using a histogram matching method to reduce radiometric differences among images caused by inconsistencies of acquisition conditions.

2.5. Pre-fire forest conditions

Forest inventory data before the Black Dragon fire were lacking. We combined 2000s forest inventory data with 1980s and 2000s Landsat TM data to map 1980s aboveground forest biomass and tree lists (i.e., lists of species and diameter for every tree), following the approaches of Zhang et al. (2018a, 2018b). We used 2000s forest inventory data and 2000s Landsat TM data as the training samples to fit a nonparametric random forest-based *k*NN model for biomass and *k*NN and Weibull parameter prediction models (WPPMs) for tree lists. Then we mapped species-level biomass and tree lists before the Black Dragon fire at 30-m resolution using 1980s Landsat TM data based on the developed biomass estimation model and tree-lists estimation model. Thus, the pre-fire forest composition (Figs. S2 and S3) represents the distribution and abundance of tree species before the 1987 Black Dragon fire.

Our imputation results (Figs. S2 and S3) conformed to previous studies and field observations. The total tree density (ranging from 400 to 2500 trees/ha, Fig. S2) and aboveground biomass (62.4 ± 22.76 Mg/ha, Fig. S3) were close to the values reported by Zhai et al. (1990), Hu et al. (2015), and Fang et al. (2001) for northeastern China. Moreover, our estimates of the species distribution (Figs. S2 and S3) were consistent with the environmental niches of tree species. Larch, the representative Siberian boreal tree species, is distributed most widely since it can endure extremely cold winters and a short growing season, and it can grow in both well-drained and boggy sites due to its shallow roots (Xu, 1998; Kajimoto et al., 2003; Yang et al., 2014). White birch is also distributed widely in the area but is less adaptable to shade and humid environments and typically has less biomass than larch (Xu, 1998). Aspen requires warmer temperatures and higher soil fertility and is negatively correlated with elevation (Xu, 1998). Scots pine has high tolerance of drought and low temperatures and consequently was mainly distributed on the sunny slopes and ridges of the northern part of our study area (Zhu et al., 2006). Mongolian oak and black birch were mainly distributed in the southeast of the area since they thrive in areas with higher temperatures (Xu, 1998). Spruce grows under cold environments and therefore was mainly mapped in areas of relatively high elevation of the northern area. Willow requires sufficient humidity to survive and is therefore widespread along rivers, which are fed by water from the glaciers and snows of the high surrounding mountains. These evaluations ensured the subsequent reconstructions of forest recovery rate and trajectories bear high realism (Temperli et al., 2013).

2.6. Landscape model parameterization

We used the LANDIS PRO forest landscape model to simulate forest landscape changes and reconstruct tree species recovery trajectories after the Black Dragon fire. The model tracks the number (density) of each tree species by age cohort (size class) at the pixel level (i.e., 100 m resolution in this study) and simulates species-, stand-, and landscape-scale processes over large spatial and temporal extents (Wang et al. 2013, 2014abib_Wang_et_al_2013bib_Wang_et_al_2014a). We used the succession module in LANDIS PRO to simulate individual tree establishment, growth, resprouting, and mortality at the species level, resources competition, self-thinning and seedling establishment at stand level, and seed dispersal at the landscape level. Establishment success is determined by species-specific biological traits, such as shade tolerance, and suitability to establish under the other environmental conditions besides shade. Mortality is determined by longevity (i.e., maximum lifespans), competition, and disturbances. Other landscape-scale processes (i.e., natural and anthropogenic disturbances) were simulated by independent modules (e.g., fire, harvesting, and fuel treatments are simulated using the fire, harvest, and fuel modules, respectively). Forest change is determined by the interactions of species-, stand-, and landscape-scale processes.

We modeled the eight most common tree species, which accounted for approximately 95% of stand volume in this study region. Tree species life history attributes included longevity, age of reproductive maturity, shade tolerance, fire tolerance, seed dispersal distance, maximum tree diameter, maximum stand density index, and number of potential germination seeds (Table 1). LANDIS PRO does not require climate and soil parameters; however, it requires species establishment probability (SEP) and maximum growing space occupied (MGSO) by land type, which delineates heterogeneous landscapes into smaller but relatively homogeneous land type units. Within each land type unit, resource availability represented by the MGSO and SEP is assumed to be homogeneous. For this study, SEP and MGSO were derived from an ecosystem process model LINKAGES 3.0 (Dijak et al., 2017) for each land type (see supplement).

2.7. Black Dragon fire and its implementation in LANDIS PRO

The spatial pattern and variability of burn severity strongly influences vegetation response, forest structure, and post-fire successional trajectories (Halofsky et al., 2011). The burn severity map of the Black Dragon fire used in this study was extracted based on the remote sensing classification from a relationship between normalized burn ration (NBR) and composite burn index (CBI) (Xu et al., 2020). The burn severity explicitly accounted for different levels of tree mortality that are important for post-fire forest succession: unburned (no sign of fire effects, NBR > 585), low severity (252 < NBR < 585), moderate severity (53 < NBR < 252), and high severity (NBR < 53).

The simulation of fire is treated as a stochastic process in the LANDIS PRO Fire module. However, there was no guarantee that the Black Dragon fire would occur in 1987 in our simulation. Thus, we mimicked this specific fire event, and its effects using the LANDIS PRO Fuel module (He et al., 2004), which can deterministically specify how live fuel loads are reduced (corresponding to tree mortality detected for each burn severity class) in fuel reduction treatments. Post-fire live tree mortality was modeled using a logistic regression equation (Equation (1) where P is probability of mortality following fire, β_i are model coefficients determining fire tolerance, X_1 is tree diameter (cm), and X_2 is height of bark charring (m) analogously for burn severity) based on previous studies (Woolley et al., 2012; Fraser et al., 2019). We divided our study area into four fuel management areas based on the four fire severity classes (Xu et al., 2020). Initial model coefficients for each species were defined based on the species fire tolerance (Fraser et al., 2019).

$$P = \left(1 + e^{-(\beta_0 + \beta_1 X_1 + \beta_2 X_2)}\right)^{-1} \quad \text{Equation (1)}$$

Table 1
Individual tree species biological traits used in LANDIS PRO in the boreal forests of China.

Major species	Longevity (years)	Maturity age (years)	Shade tolerance [a]	Fire tolerance [b]	Maximum seeding distance/m	Maximum DBH/cm	Maximum stand density (trees/ha)	Potential germination seeds [c]
Larch *(Larix gmelinii)*	300	20	2	4	150	55	600	10
Scots pine *(Pinus sylvestris)*	250	25	2	3	200	60	560	20
White birch *(Betula platyphylla)*	150	15	1	3	2000	30	690	30
Aspen (Populus davidiana)	120	10	1	4	2000	50	680	30
Spruce (Picea koraiensis)	300	30	4	3	150	60	520	10
Willow (*Chosenia arbutifolia*)	250	12	2	5	2000	50	780	20
Black birch (*Betula davurica)*	150	15	2	3	800	50	750	25
Mongolian oak *(Quercus mongolica)*	300	20	3	5	200	95	600	20

Species data were obtained from the Scientific Database of China Plant Species (http://db.kib.ac.cn) and previous studies (Li et al., 2013; Luo et al., 2015). [a, b] Shade/fire tolerance classes 1–5: 1 = least tolerant, 5 = most tolerant.
[c] Mean number of potential germinating seeds produced/mature tree/year.

2.8. Model calibration and results validation

Forest inventory data in unburned area were available for years 2000, 2010, and 2015. The 2000, 2010 data were used to calibrate tree species parameters while the 2015 data were used to validate the simulated results. Forest inventory data in burned areas were only available for years 2000 and 2015. The 2000 data were used to calibrate fire parameters and the 2015 data were used to validate the simulated fire effects (Fig. 2a and b). Only simulated trees with DBH >5 cm and forest inventory data that were in the study areas with no evidence of disturbance (e.g., logging, insects, disease, and fire) after 1987 were used in the calibration and validation processes.

Model fit can be assessed using the difference between the simulated results and true values, while overfitting can result in deterioration in prediction accuracy (Lever et al., 2016). In this study, to calibrate tree species parameters, we iteratively adjusted the age-DBH relationship and available seeds for each species by land types until the differences between simulated density and basal area by species and the forest inventory were not significant (no differences based on a one-way analysis of variance (ANOVA) test ($p > 0.05$)) at 2000 and 2010, to ensure that the these parameters realistically represented the actual forests in our study area. We validated the simulated results at the landscape scale by stratifying the simulation results and forest inventory data into subecoregions based on the ecoregion classification of Xu (1998) and soil types (Fig. S4), because resource availability and species assemblages were relatively homogeneous within a subecoregion and heterogeneous among subecoregions in LANDIS PRO for undisturbed forests. Specifically, we compared the simulated mean basal area and tree density of all cells to the observed mean values of all plots for each subecoregion in 2015 by using paired *t*-test to evaluate the overall accuracy, and the square of the Pearson correlation (R^2) and root mean square deviation (RMSD) for each species. RMSD was based on squared simulation errors and thus was sensitive to outliers.

To calibrate fire parameters, we iteratively adjusted fuel model coefficients for each species fire tolerance class and height of bark charring for each burn severity until the comparison between simulated density and basal area by species and the forest inventory data passed the significance test (no differences based on an ANOVA test ($p > 0.05$)) at 2000. We validated the simulation results for each burn severity class at site scale by extracting simulated results from raster cells corresponding to the forest inventory plot locations, because heterogeneous post-fire tree species recovery patterns overrode environmental heterogeneity delineated by subecoregion. Specifically, we compared basal area and tree density within extracted raster cells with observed values in inventory plots for each burn severity class at 2015 by using two sample *t*-test to evaluate the accuracy of simulated post-fire recovery. All statistical analyses were performed using R statistical software (R Core Team, 2015).

2.9. Post-fire tree planting simulation

Large-scale tree plantings in the years immediately after the fire were implemented in each Forest Bureau. Thus, we simulated planting using the LANDIS PRO Harvest module (Fraser et al., 2013). The planting management units in this study were constructed based on the burn severity map of the 1987 Black Dragon fire, Forest Bureau boundaries, and harvest management units to capture the variation in planting practices across the region. We parameterized the percent area and number of trees planted every two years for each management unit based on forest management records from the China National Forest Inventory third tier data (http://www.cfsdc.org) and previous studies (Yang et al., 1998; Chen et al., 2014). Only coniferous species of larch and Scots pine were planted in the high burn severity area (70% larch + 30% pine) with a regular plant spacing (1.5 m × 1.5 m or 1.5 m × 2 m) according to field conditions (Chen et al., 2014). By the end of the 1990s, less than 10% of the burned forests were managed with planting (Yang et al., 1998).

3. Results

3.1. Results validation

Model simulations showed high agreement in the magnitude and time of observed basal area and density from unburned forests at the landscape scale (paired t-tests, $p > 0.05$). R^2 (>0.8) is high and RMSD is low for both basal area and density for all species (Fig. 3). The comparisons of different species demonstrated that dominant tree species (larch and white birch) had relatively higher accuracy than other species. The simulation accuracy for tree density was higher than for basal area because the density in the model was largely determined by a single parameter (available seeds), while the basal area was affected by the species age-DBH relationship that introduced additional uncertainties into estimation. Overall, our results indicated that the simulated forest development was consistent with the actual forest dynamics, and simulated density had higher accuracy than simulated basal area.

Comparison between simulated data and observed data showed that post-fire forest composition and structure closely represented the real forest composition and structure at different burn severity classes in 2015 (for all species and severities, two sample *t*-test, $p > 0.05$) (Fig. 4). Our results indicated that the simulated post-fire forest development captured current forest composition and structure after the Black Dragon fire and thus the simulated fire-caused tree species mortality could be close to the real tree species mortality of the Black Dragon fire.

The observed and simulated density of conifer and broadleaf species in burned areas showed similar patterns in relation to distance to live-tree edges (trees mortality rate $< 90\%$ by the Black Dragon fire) (Fig. 5). Post-fire conifer density showed a decline with increasing distance to the live tree edge and was almost absent in the interior of high burn severity patches in 2015 (Fig. 5a). Post-fire broadleaf density was high across the whole high severity area and had an opposite trend of density versus distance relationship compared with conifer species (Fig. 5b). The self-thinning among competing trees led to a decrease in tree density near seed sources. The evaluation results increased our confidence in the ability of the calibrated LANDIS PRO model to explore the long-term fire effects and post-fire forest recovery.

3.2. The Black Dragon fire effects and post-fire forest recovery trajectories

Tree mortality and post-fire recovery varied greatly among burn severities and tree species (Fig. 6 and S5). Mortalities of conifer and broadleaf species were both positively related to burn severity and were very high in areas with moderate and high burn severity (Fig. 6a and b). Approximately 50%–90% of conifer and almost 100% of broadleaf stems died in areas of moderate and high burn severity. Nevertheless, recruitment of broadleaf trees was abundant in moderate and high severity burned areas. The post-fire density of broadleaf species gradually increased over the first 12 years, then sharply peaked between 2005 and 2010 (12,000 and 10,000 trees/ha), and finally decreased to 10,000 and 7000 trees/ha by 2015 in high and moderate burn severity areas, respectively. The changes in density, basal area, and biomass over time in unburned and low severity areas were not significant (Fig. 6b). The post-fire density of conifer species showed a low rate of increase compared to broadleaf species (Fig. 6a). The post-fire basal areas of conifer and broadleaf species both showed increasing trends throughout the simulation years under all burn severities (Fig. 6c and d). For broadleaf species, the basal area has recovered to, and even exceeded pre-fire levels, although aboveground biomass always remained lower than pre-fire levels (Fig. 6c–f). For conifer species, both basal area and biomass remained below pre-fire levels, but the recovery rate in low burn severity was fastest (Fig. 6c and e). With time, the percentage of coniferous species decreased in high and moderate severity burned areas, but no significant changes occurred in low severity and unburned

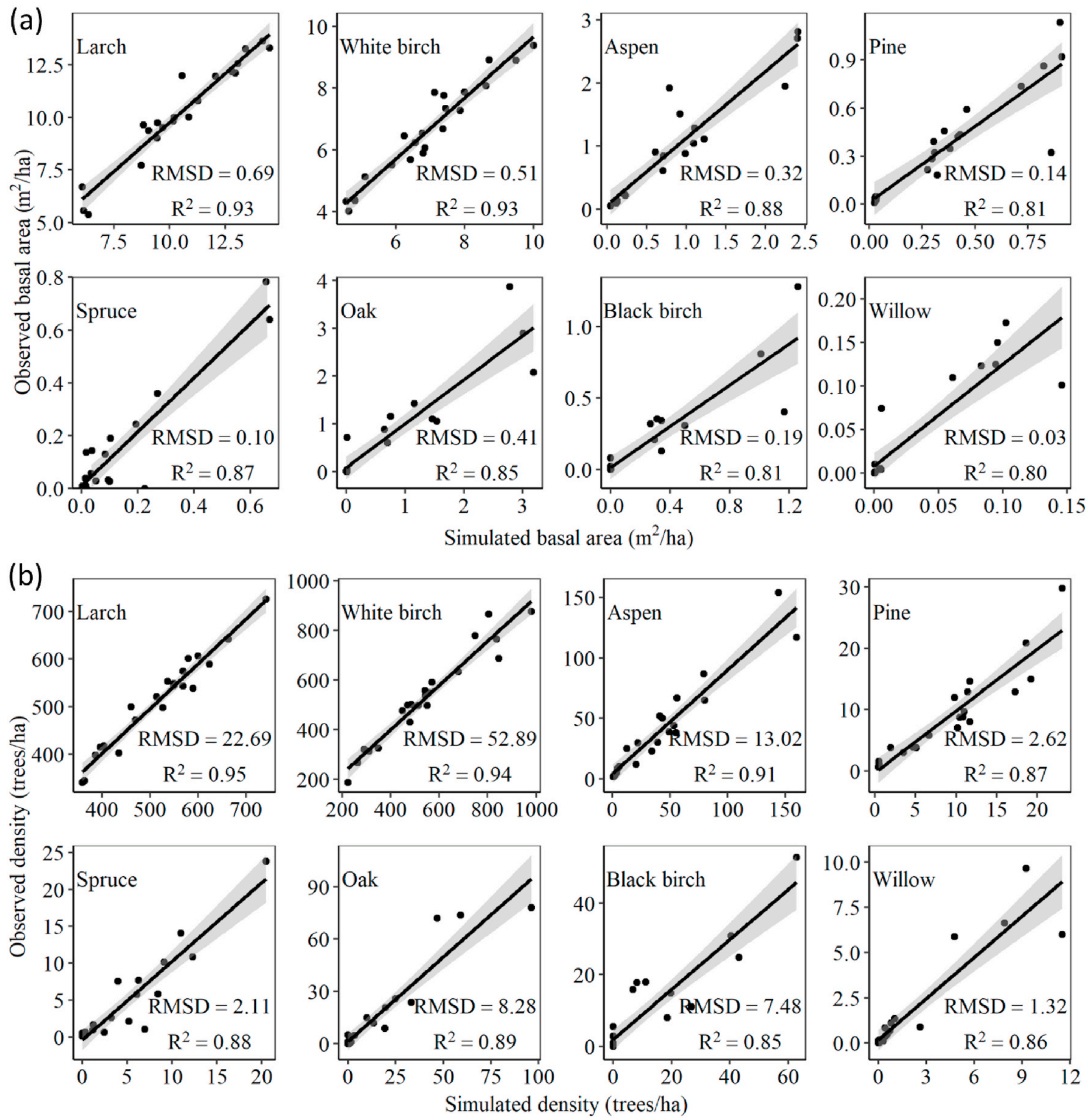

Fig. 3. Scatterplots of simulated versus forest inventory density (a) and basal area (b) of eight species at the landscape scale in 2015 (n = 21). The black line is the regression line and the grey shaded area represents 95% confidence intervals. RMSD: root mean squared deviation.

areas (Fig. 7a). The percent of coniferous species in high and moderate severity burned areas was far less than the value in unburned forests at 2015, but the edges of these burned patches showed a composition recovery sign with larger conifer percentages than the interior (Fig. 7).

4. Discussion

We presented a spatially explicit framework to reconstruct post-megafire forest recovery through integrating a forest landscape model (FLM) and remote sensing and field inventory data. Reconstruction results showed that burn severity affected the relative dominance of broadleaf vs. conifer species in burned stands with probable effects on subsequent canopy dominance. In high severity burned areas, broadleaf species (e.g., white birch) rapidly emerged despite the large burn size, while regeneration of coniferous species (e.g., larch) was minimal in the interior of the burned patches. This pattern matches expectations because white birch can rapidly regenerate either by resprouting from stumps or roots that survived fires or by long distance seed dispersal (e.g., >1000 m). However, the regeneration of larch depends on the seeds from surviving trees and a relatively short seed dispersal distance (<400 m) (Xu, 1998). Thirty years after the megafire, the broadleaf species fully recovered, and white birch stands went into the self-thinning stage in the interior of the high severity burned area as the newly established trees matured. However, coniferous species were still in the initial stand development stage. In contrast, more conifers than broadleaf species regrew in the low-severity burned areas, where canopies provided suitable conditions for the relatively more shade-tolerant conifers and where sufficient seeds from surviving trees had a higher chance to reach fire-released areas in the low-severity burned patches. The comparison of pre- and post-fire tree composition in the burned patches indicated that self-replacement succession was likely to occur in areas that burned with low severity, whereas high severity burned areas are more likely to shift forest successional trajectories away from conifer self-replacement to pathways with greater broadleaf dominance, a finding that is reported in other post-fire studies (Johnstone and Chapin, 2006; Johnstone et al., 2010; Cai et al., 2013). Our reconstructed trajectories of post-megafire forest recovery were well supported by known data and empirical knowledge of forest stand development after large-scale disturbances (Oliver et al., 1996; Turner et al., 1998; Kurkowski et al., 2008), suggesting that our model framework is effective in spatially reconstructing

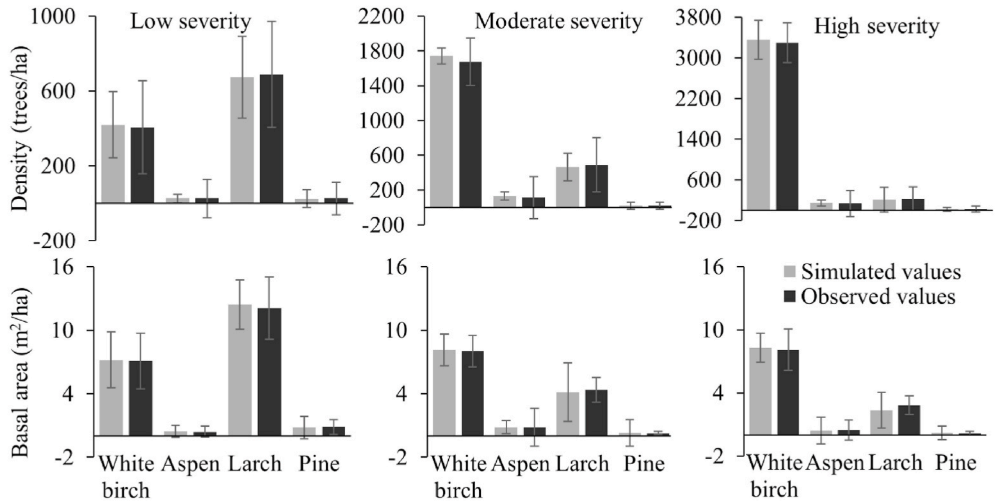

Fig. 4. Comparison of simulated tree species density (a) and basal area (b) with inventory data by burn severities of the Black Dragon fire at 2015. Error bars are marked as ± 1 standard deviation (n = 584, 366, and 355 for low, moderate, and high severity area, respectively).

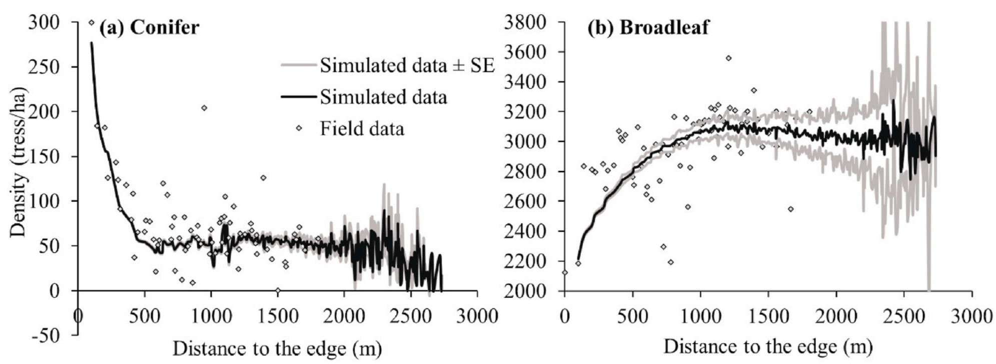

Fig. 5. Post-fire 28-year coniferous (a) and broadleaf (b) density in high burned area as a function of Euclidean distance to 1987 live-tree edge (trees mortality rate < 90%) after the Black Dragon fire. The black lines are simulated means and grey lines are ±1 standard error (SE). The points are observed values from field inventory data.

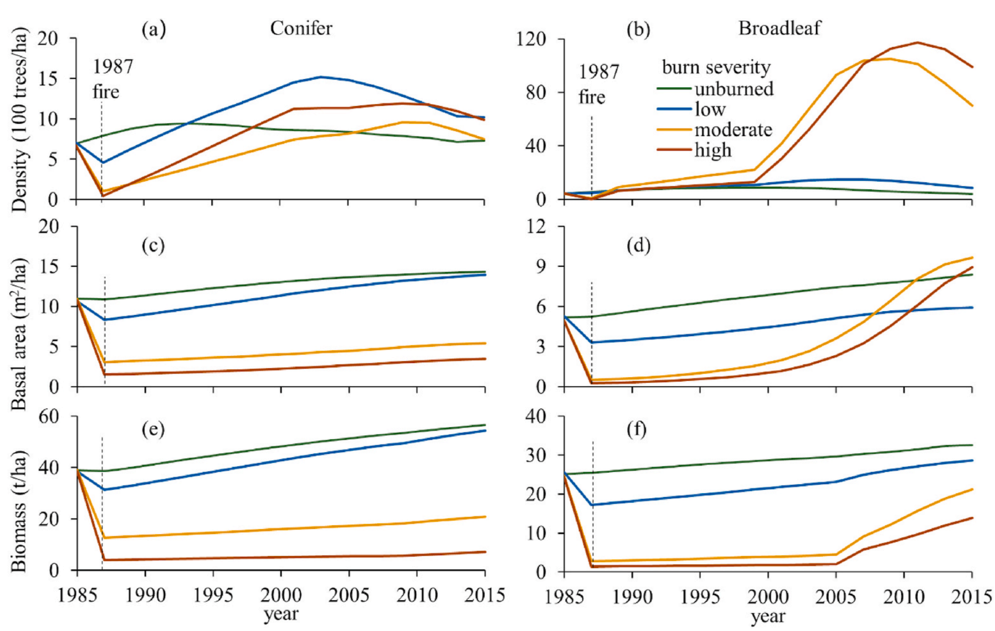

Fig. 6. Tree species recovery trajectories over time for each burn severity following the 1987 Black Dragon fire: the trajectories of conifer species recovery in density (a), basal area (c), and biomass (e), and broadleaf species recovery in density (b), basal area (d), and biomass (f) from 1985 to 2015.

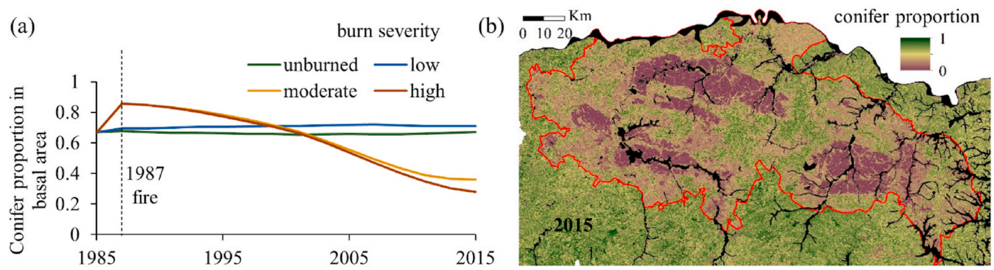

Fig. 7. Tracking changes in species composition. (a) Trajectories of conifer proportion in basal area for each burn severity from 1985 to 2015. (b) Map of conifer proportion in basal area in 2015. Red line denotes perimeter of Black Dragon fire. (For interpretation of the references to colour in this figure legend, the reader is referred to the Web version of this article.)

post-megafire historical forest conditions.

Validating simulation results from FLMs is critical in quantifying the reliability and credibility of landscape reconstructions. Our framework of reconstructing the spatiotemporal history of post-megafire forest conditions provided not only the spatial pattern and dynamics at the landscape scale, but also detailed stand attributes such as basal area, tree density, and age classes by species. We validated the simulated stand attributes with the contemporary inventory data. Our simulated tree mortality rates were close to the estimates of tree mortality rates from field inventories within different burn severity classes of the Black Dragon fire (Luo, 2002). The simulated post-fire density and biomass were comparable to the field observations reported by Wang et al. (2001), Wang et al. (2003), and Hu et al. (2016) for the same fire and other post-fire studies in boreal forests after similar recovery periods (Johnstone et al., 2004; Alexander et al., 2012; Cai et al., 2013). Our validation results from current forest inventory data demonstrated the calibrated model performed well and ensured that the model was a reasonable and reliable platform for subsequent applications to quantify the effects of megafires on forest composition and landscape succession.

A notable benefit of our framework is that, once calibrated, the model is highly scalable and can be applied to filling the gaps where inventory data are not available to assess recovery trajectories across the whole landscape. This method offers an approach to augment traditional uses of forest inventory data in post-fire studies. Our approach realistically captures the heterogeneity of post-fire recovery process in both time and space (Figs. 5 and 6, S5). In contrast, forest inventories, when applied alone, have generally focused on fixed plots or time periods and on describing entire landscapes, which limit their ability to constrain the impacts of heterogeneity on timber volumes and carbon stocks (e.g., Kashian et al., 2005). Furthermore, inventory approaches can suffer from biased sampling design. For example, Wang et al. (2001) and Hu et al. (2016) conducted studies near the live-tree edges due to the logistical limitations, observed a higher biomass recovery than we did in this study, and thus overestimated the post-fire recovery status. They assumed that the mature forests were representative of the forests in this region prior to the 1987 fire. However, through historical forest conditions reconstruction, we found that pre-fire forests in this area were younger than Wang et al. (2001) and Hu et al. (2016) assumed, because forests in this region were affected by historical harvesting and fires, which resulted in relatively young stands with most trees between 40 and 60 years old. These studies may have overestimated pre-fire forest biomass and consequently biomass loss due to the Black Dragon fire, while our simulated biomass loss was closer to the estimated values from the traditional bottom-up method (Xu et al., 2020). This highlights the importance of our approach that reconstruction of the entire historical landscape reduced the biases from field sampling.

This framework can be applied to assess the legacy effects of a megafire over long time periods (i.e., decades to centuries). While previous empirical and field-based studies documented legacy effects (e.g., Downing et al., 2019), such effects can persist for decades to centuries (Seidl et al., 2012) and thus require long-term assessment. Our framework can be further applied to projecting how forest landscapes respond to future megafires, which are expected to increase under warming climate and increased fuel accumulation from fire exclusion policies (Chang et al., 2007; Flannigan et al., 2009; Liu et al., 2012).

Our framework can also be used to examine alternative management and disturbance scenarios. Managers could use the framework to evaluate forest resistance, rate of recovery, and the time to return to predisturbance states after megafires under various management and climate scenarios as well as to study the effect of alternative managements on mitigating future megafire risk. For example, reforestation is increasingly used to assist forest restoration and improve resilience, especially under warming climate as conifer forests will be increasingly regeneration limited with intensifying fire regimes (Hof et al., 2017; North et al., 2019). Different reforestation strategies (e.g., planting intensity and spatial assignment) can be evaluated with FLMs (Wang et al. 2006a, 2006bbib_Wang_et_al_2006abib_Wang_et_al_2006b). Researchers can also use this framework to evaluate the response of forest landscapes to other forest disturbances such as drought, insect, and harvest under different environmental settings.

Declaration of competing interest

The authors declare that they have no known competing financial interests or personal relationships that could have appeared to influence the work reported in this paper.

Acknowledgements

This research was funded by the National Biologic Carbon Sequestration Assessment Program under the U.S. Geological Survey Climate and Land Use Mission Area. Any use of trade, firm, or product names is for descriptive purposes only and does not imply endorsement by the U. S. Government.

Xu, W., He H.S., Fraser, J.S., Hawbaker, T.J., Henne, P.D., Duan, S. and Zhu, Z, 2020, Data release for: Spatially explicit reconstruction of post-megafire forest recovery through landscape modeling, U.S. Geological Survey data release, https://doi.org/10.5066/P9HRHBXZ.

Appendix A. Supplementary data

Supplementary data to this article can be found online at https://doi.org/10.1016/j.envsoft.2020.104884.

References

Alexander, H.D., Mack, M.C., Goetz, S., Loranty, M.M., Beck, P.S.A., Earl, K., Zimov, S., Davydov, S., Thompson, C.C., 2012. Carbon accumulation patterns during post-fire succession in cajander larch (Larix cajanderi) forests of Siberia. Ecosystems 15, 1065–1082.

Bonnet, V.H., Schoettle, A.W., Shepperd, W.D., 2005. Postfire environmental conditions influence the spatial pattern of regeneration for Pinus ponderosa. Can. J. For. Res. 35, 37–47.

Bowman, D.M.J.S., et al., 2009. Fire in the earth system. Science 324, 481–484.

Boychuk, D., Perera, A.H., Ter-Mikaelian, M.T., Martell, D.L., Li, C., 1997. Modelling the effect of spatial scale and correlated fire disturbances on forest age distribution. Ecol. Model. 95, 145–164.

Bradstock, R.A., 2008. Effects of large fires on biodiversity in southeastern Australia: disaster or template for diversity? Int. J. Wildland Fire 17, 809–822.

Broncano, M.J., Retana, J., 2004. Topography and forest composition affecting the variability in fire severity and post-fire regeneration occurring after a large fire in the Mediterranean basin. Int. J. Wildland Fire 13, 209–216.

Cai, W.H., Yang, J., Liu, Z., Hu, Y., Weisberg, P.J., 2013. Post-fire tree recruitment of a boreal larch forest in Northeast China. For. Ecol. Manag. 307, 20–29.

Cai, W.H., Liu, Z.H., Yang, Y.Z., Yang, J., 2018. Does environment filtering or seed limitation determine post-fire forest recovery patterns in boreal larch forests? Front. Plant Sci. 9, 1318.

Chang, Y., He, H.S., Bishop, I., Hu, Y., Bu, R., Xu, C., Li, X., 2007. Long-term forest landscape responses to fire exclusion in the Great Xing'an Mountains, China. Int. J. Wildland Fire 16, 34–44.

Chang, Y., He, H.S., Hu, Y., Bu, R., Li, X., 2008. Historic and current fire regimes in the Great Xing'an Mountains, northeastern China: implications for long-term forest management. For. Ecol. Manag. 254, 445–453.

Chen, W., Moriya, K., Sakai, T., Koyama, L., Cao, C.X., 2014. Post-fire forest regeneration under different restoration treatments in the Greater Hinggan Mountain area of China. Ecol. Eng. 70, 304–311.

Chu, T.A., Guo, X.L., 2014. Remote sensing techniques in monitoring post-fire effects and patterns of forest recovery in boreal forest regions: a review. Rem. Sens. 6, 470–520.

Collins, B.M., Roller, G.B., 2013. Early forest dynamics in stand-replacing fire patches in the northern Sierra Nevada, California, USA. Landsc. Ecol. 28, 1801–1813.

Crotteau, J.S., Varner, J.M., Ritchie, M.W., 2013. Post-fire regeneration across a fire severity gradient in the southern Cascades. For. Ecol. Manag. 287, 103–112.

Cuevas-Gonzalez, M., Gerard, F., Balzter, H., Riano, D., 2009. Analysing forest recovery after wildfire disturbance in boreal Siberia using remotely sensed vegetation indices. Global Change Biol. 15, 561–577.

Davis, K.T., Higuera, P.E., Sala, A., 2018. Anticipating fire-mediated impacts of climate change using a demographic framework. Funct. Ecol. 32, 1729–1745.

Dijak, W.D., Hanberry, B.B., Fraser, J.S., He, H.S., Wang, W.J., Thompson, F.R., 2017. Revision and application of the LINKAGES model to simulate forest growth in central hardwood landscapes in response to climate change. Landsc. Ecol. 32, 1365–1384.

Downing, W.M., Krawchuk, M.A., Meigs, G.W., Haire, S.L., Coop, J.D., Walker, R.B., Whitman, E., Chong, G., Miller, C., 2019. Influence of fire refugia spatial pattern on post-fire forest recovery in Oregon's Blue Mountains. Landsc. Ecol. 34, 771–792.

Eidenshink, J., Schwind, B., Brewer, K., Zhu, Z.-L., Quayle, B., Howard, S., 2007. A project for monitoring trends in burn severity. Fire ecol. 3, 3–21.

Epting, J., Verbyla, D., Sorbel, B., 2005. Evaluation of remotely sensed indices for assessing burn severity in interior Alaska using Landsat TM and ETM+. Remote Sens. Environ. 96, 328–339.

Fang, J.Y., Chen, A.P., Peng, C.H., Zhao, S.Q., Ci, L., 2001. Changes in forest biomass carbon storage in China between 1949 and 1998. Science 292, 2320–2322.

Flannigan, M.D., Krawchuk, M.A., de Groot, W.J., Wotton, B.M., Gowman, L.M., 2009. Implications of changing climate for global wildland fire. Int. J. Wildland Fire 18, 483–507.

Fraser, J.S., He, H.S., Shifley, S.R., Wang, W.J., Thompson III, F.R., 2013. Simulating stand-level harvest prescriptions across landscapes: LANDIS PRO harvest module design. Can. J. For. Res. 43, 972–978.

Fraser, J.S., Wang, W.J., He, H.S., Thompson, F.R., 2019. Modeling post-fire tree mortality using a logistic regression method within a forest landscape model. Forests 10.

French, N.H.F., Kasischke, E.S., Hall, R.J., Murphy, K.A., Verbyla, D.L., Hoy, E.E., Allen, J.L., 2008. Using Landsat data to assess fire and burn severity in the North American boreal forest region: an overview and summary of results. Int. J. Wildland Fire 17, 443–462.

García, M.L., Caselles, V., 1991. Mapping burns and natural reforestation using Thematic Mapper data. Geocarto Int. 6, 31–37.

Gitas, I., Mitri, G., Veraverbeke, S., Polychronaki, A., 2012. Advances in remote sensing of post-fire vegetation recovery monitoring—a review. Remote Sens. Biomass Princ. Appl. 1, 334.

Glenn, E.P., Huete, A.R., Nagler, P.L., Nelson, S.G., 2008. Relationship between remotely-sensed vegetation indices, canopy attributes and plant physiological processes: what vegetation indices can and cannot tell us about the landscape. Sensors 8, 2136–2160.

Greene, D.F., et al., 2007. The reduction of organic-layer depth by wildfire in the North American boreal forest and its effect on tree recruitment by seed. Can. J. For. Res. 37, 1012–1023.

Halofsky, J.E., et al., 2011. Mixed-severity fire regimes: lessons and hypotheses from the Klamath-Siskiyou Ecoregion. Ecosphere 2.

Harvey, B.J., Donato, D.C., Turner, M.G., 2016. High and dry: post-fire tree seedling establishment in subalpine forests decreases with post-fire drought and large stand-replacing burn patches. Global Ecol. Biogeogr. 25, 655–669.

He, H.S., 2008. Forest landscape models: definitions, characterization, and classification. For. Ecol. Manag. 254, 484–498.

He, H.S., Shang, B.Z., Crow, T.R., Gustafson, E.J., Shifley, S.R., 2004. Simulating forest fuel and fire risk dynamics across landscapes - LANDIS fuel module design. Ecol. Model. 180, 135–151.

Hof, A.R., Dymond, C.C., Mladenoff, D.J., 2017. Climate change mitigation through adaptation: the effectiveness of forest diversification by novel tree planting regimes. Ecosphere 8, e01981.

Hu, H., Luo, B., Wei, S., 2015. Estimating biological carbon storage of five typical forest types in the Daxing'anling Mountain, Heilongjia, China. Acta Ecol. Sin. 35, 1–21.

Hu, X., Zhu, J., Wang, C., Zheng, T., Wu, Q., Yao, H., Fang, J., 2016. Impacts of fire severity and post-fire reforestation on carbon pools in boreal larch forests in Northeast China. J. Plant Ecol. 9, 1–9.

Huang, C., He, H.S., Liang, Y., Wu, Z.W., Hawbaker, T.J., Gong, P., Zhu, Z.L., 2018. Long-term effects of fire and harvest on carbon stocks of boreal forests in northeastern China. Ann. For. Sci. 75.

Idris, M.H., Kuraji, K., Suzuki, M., 2005. Evaluating vegetation recovery following large-scale forest fires in Borneo and northeastern China using multi-temporal NOAA/AVHRR images. J. For. Res. 10, 101–111.

Johnstone, J.F., et al., 2016. Changing disturbance regimes, ecological memory, and forest resilience. Front. Ecol. Environ. 14, 369–378.

Johnstone, J.F., Chapin, F.S., 2006. Effects of soil burn severity on post-fire tree recruitment in boreal forest. Ecosystems 9, 14–31.

Johnstone, J.F., Chapin, F.S., Foote, J., Kemmett, S., Price, K., Viereck, L., 2004. Decadal observations of tree regeneration following fire in boreal forests. Can. J. For. Res. 34, 267–273.

Johnstone, J.F., Hollingsworth, T.N., Chapin, F.S., Mack, M.C., 2010. Changes in fire regime break the legacy lock on successional trajectories in Alaskan boreal forest. Global Change Biol. 16, 1281–1295.

Ju, J.C., Roy, D.P., 2008. The availability of cloud-free Landsat ETM plus data over the conterminous United States and globally. Remote Sens. Environ. 112, 1196–1211.

Kajimoto, T., Matsuura, Y., Osawa, A., Prokushkin, A.S., Sofronov, M.A., Abaimov, A.P., 2003. Root system development of Larix gmelinii trees affected by micro-scale conditions of permafrost soils in central Siberia. Plant Soil 255, 281–292.

Kashian, D.M., Turner, M.G., Romme, W.H., Lorimer, C.G., 2005. Variability and convergence in stand structural development on a fire-dominated subalpine landscape. Ecology 86, 643–654.

Keane, R.E., Agee, J.K., Fule, P., Keeley, J.E., Key, C., Kitchen, S.G., Miller, R., Schulte, L. A., 2008. Ecological effects of large fires on US landscapes: benefit or catastrophe? Int. J. Wildland Fire 17, 696–712.

Kemp, K.B., Higuera, P.E., Morgan, P., Abatzoglou, J.T., 2019. Climate will increasingly determine post-fire tree regeneration success in low-elevation forests, Northern Rockies, USA. Ecosphere 10, e02568.

Key, C., Benson, N., 2005. Landscape Assessment: Ground Measure of Severity; the Composite Burn Index, and Remote Sensing of Severity, the Normalized Burn Index and Remote Sensing of Severity, the Normalized Burn Ratio. FIREMON: Fire Effects Monitoring and Inventory System. USDA Forest Service, Rocky Mountain Research Station, Ogden, UT, pp. 1–51.

Kurkowski, T.A., Mann, D.H., Rupp, T.S., Verbyla, D.L., 2008. Relative importance of different secondary successional pathways in an Alaskan boreal forest. Can. J. For. Res.-Revue Canadienne De Recherche Forestiere 38, 1911–1923.

Lecomte, N., Simard, M., Fenton, N., Bergeron, Y., 2006. Fire severity and long-term ecosystem biomass dynamics in coniferous boreal forests of eastern Canada. Ecosystems 9, 1215–1230.

Lever, J., Krzywinski, M., Altman, N., 2016. Points of significance: model selection and overfitting. Nat. Methods 13, 703.

Li, X., He, H.S., Wu, Z., Liang, Y., Schneiderman, J.E., 2013. Comparing effects of climate warming, fire, and timber harvesting on a boreal forest landscape in northeastern China. PloS One 8, e59747.

Liu, Z.H., Yang, J., Chang, Y., Weisberg, P.J., He, H.S., 2012. Spatial patterns and drivers of fire occurrence and its future trend under climate change in a boreal forest of Northeast China. Global Change Biol. 18, 2041–2056.

Luo, J., 2002. Influence of forest fire disaster on forest ecosystem in Great Xing'anling (in Chinese). J. Beijing For. Univ. 24, 101–107.

Luo, X., He, H.S., Liang, Y., Wu, Z., 2015. Evaluating simulated effects of succession, fire, and harvest for LANDIS PRO forest landscape model. Ecol. Model. 297, 1–10.

Luo, Y.Q., Ogle, K., Tucker, C., Fei, S.F., Gao, C., LaDeau, S., Clark, J.S., Schimel, D.S., 2011. Ecological forecasting and data assimilation in a data-rich era. Ecol. Appl. 21, 1429–1442.

Masek, J.G., Vermote, E.F., Saleous, N.E., Wolfe, R., Hall, F.G., Huemmrich, K.F., Gao, F., Kutler, J., Lim, T.K., 2006. A Landsat surface reflectance dataset for North America, 1990-2000. Geosci. Rem. Sens. Lett. IEEE 3, 68–72.

Miller, J.D., Thode, A.E., 2007. Quantifying burn severity in a heterogeneous landscape with a relative version of the delta Normalized Burn Ratio (dNBR). Remote Sens. Environ. 109, 66–80.

Miller, C., Ager, A.A., 2013. A review of recent advances in risk analysis for wildfire management. Int. J. Wildland Fire 22, 1–14.

Millington, J.D., Wainwright, J., Perry, G.L., Romero-Calcerrada, R., Malamud, B.D., 2009. Modelling Mediterranean landscape succession-disturbance dynamics: a landscape fire-succession model. Environ. Model. Software 24, 1196–1208.

North, M.P., Stevens, J.T., Greene, D.F., Coppoletta, M., Knapp, E.E., Latimer, A.M., Restaino, C.M., Tompkins, R.E., Welch, K.R., York, R.A., Young, D.J., 2019. Tamm Review: reforestation for resilience in dry western US forests. For. Ecol. Manag. 432, 209–224.

Oliver, C.D., Larson, B.C., Oliver, C., 1996. Forest Stand Dynamics. Wiley, New York.

Petrie, M.D., Wildeman, A.M., Bradford, J.B., Hubbard, R.M., Lauenroth, W.K., 2016. A review of precipitation and temperature control on seedling emergence and establishment for ponderosa and lodgepole pine forest regeneration. For. Ecol. Manag. 361, 328–338.

R Core Team, 2015. R: A Language and Environment for Statistical Computing (Version 3.2.2). R Foundation for Statistical Computing, Vienna, Austria. Retrieved from. http://www.R-project.org/.

Savage, M., Mast, J.N., Feddema, J.J., 2013. Double whammy: high-severity fire and drought in ponderosa pine forests of the Southwest. Can. J. For. Res.-Revue Canadienne De Recherche Forestiere 43, 570–583.

Seidl, R., Rammer, W., Scheller, R.M., Spies, T.A., 2012. An individual-based process model to simulate landscape-scale forest ecosystem dynamics. Ecol. Model. 231, 87–100.

Seidl, R., Rammer, W., Spies, T.A., 2014. Disturbance legacies increase the resilience of forest ecosystem structure, composition, and functioning. Ecol. Appl. 24, 2063–2077.

Stephens, S.L., Burrows, N., Buyantuyev, A., Gray, R.W., Keane, R.E., Kubian, R., Liu, S., Seijo, F., Shu, L., Tolhurst, K.G., 2014. Temperate and boreal forest mega-fires: characteristics and challenges. Front. Ecol. Environ. 12, 115–122.

Temperli, C., Zell, J., Bugmann, H., Elkin, C., 2013. Sensitivity of ecosystem goods and services projections of a forest landscape model to initialization data. Landsc. Ecol. 28, 1337–1352.

Thrippleton, T., Dolos, K., Perry, G.L.W., Groeneveld, J., Reineking, B., 2014. Simulating long-term vegetation dynamics using a forest landscape model: the post-Taupo succession on Mt Hauhungatahi, North Island, New Zealand. N. Z. J. Ecol. 38, 26–U43.

Turner, M.G., Baker, W.L., Peterson, C.J., Peet, R.K., 1998. Factors influencing succession: lessons from large, infrequent natural disturbances. Ecosystems 1, 511–523.

Turner, M.G., Whitby, T.G., Tinker, D.B., Romme, W.H., 2016. Twenty-four years after the Yellowstone Fires: are postfire lodgepole pine stands converging in structure and function? Ecology 97, 1260–1273.

van Leeuwen, W.J.D., Casady, G.M., Neary, D.G., Bautista, S., Alloza, J.A., Carmel, Y., Wittenberg, L., Malkinson, D., Orr, B.J., 2010. Monitoring post-wildfire vegetation response with remotely sensed time-series data in Spain, USA and Israel. Int. J. Wildland Fire 19, 75–93.

Veraverbeke, S., Gitas, I., Katagis, T., Polychronaki, A., Somers, B., Goossens, R., 2012. Assessing post-fire vegetation recovery using red-near infrared vegetation indices: accounting for background and vegetation variability. ISPRS J. Photogrammetry Remote Sens. 68, 28–39.

Wang, C., Gower, S.T., Wang, Y., Zhao, H., Yan, P., Bond-Lamberty, B.P., 2001. The influence of fire on carbon distribution and net primary production of boreal Larix gmelinii forests in north-eastern China. Global Change Biol. 7, 719–730.

Wang, W.J., He, H.S., Fraser, J.S., Thompson, F.R., Shifley, S.R., Spetich, M.A., 2014a. Landis PRO: a landscape model that predicts forest composition and structure changes at regional scales. Ecography 37, 225–229.

Wang, W.J., He, H.S., Spetich, M.A., Shifley, S.R., Thompson, F.R., Dijak, W.D., Wang, Q., 2014b. A framework for evaluating forest landscape model predictions using empirical data and knowledge. Environ. Model. Software 62, 230–239.

Wang, W.J., He, H.S., Spetich, M.A., Shifley, S.R., Thompson, F.R., Larsen, D.R., Fraser, J. S., Yang, J., 2013. A large-scale forest landscape model incorporating multi-scale processes and utilizing forest inventory data. Ecosphere 4, 1–22.

Wang, W.J., Thompson, F.R., He, H.S., Fraser, J.S., Dijak, W.D., Jones-Farrand, T., 2019. Climate change and tree harvest interact to affect future tree species distribution changes. J. Ecol. 107, 1901–1917.

Wang, X., Li, X., Kong, F., Li, Y., Shi, B., Gao, Z., 2003. Model of vegetation restoration under natural regeneration and human interference in the burned area of northern Daxinganling. Chin. J. Appl. Ecol. 22, 30–34.

Wang, X.G., He, H.S., Li, X.Z., Chang, Y., Hu, Y.M., Xu, C.G., Bu, R.C., Xie, F.J., 2006a. Simulating the effects of reforestation on a large catastrophic fire burned landscape in northeastern China. For. Ecol. Manag. 225, 82–93.

Wang, X.G., He, H.S., Li, X.Z., Hu, Y.M., 2006b. Assessing the cumulative effects of postfire management on forest landscape dynamics in northeastern China. Can. J. For. Res. 36, 1992–2002.

Wang, Y., Zhou, Y., Yang, J., He, H., Zhu, Z., Ohlen, D., 2009. Simulation of short-term post-fire vegetation recovery by integration of LANDFIRE data products, DNBR data and LANDIS modeling. Spatial Sci. 15, 47–59.

Woolley, T., Shaw, D.C., Ganio, L.M., Fitzgerald, S., 2012. A review of logistic regression models used to predict post-fire tree mortality of western North American conifers. Int. J. Wildland Fire 21, 1–35.

Xu, H., 1998. Forest in Great Xing'an Mountains of China (In Chinese), vol. 1. Science Press, Beijing, p. 231.

Xu, H., Li, Z., Qiu, Y., 1997. Fire disturbance history in virgin forest in northern region of Daxinganling Mountains (in Chinese). Acta Ecol. Sin. 17, 337–343.

Xu, H., 1998. In: Forest in Great Xing'an Mountains of China, 1. Science Press, Beijing, p. 231. In: (In Chinese).

Xu, W., He, H.S., Hawbaker, T.J., Zhu, Z., Henne, P.D., 2020. Estimating burn severity and carbon emissions from a historic megafire in boreal forests of China. Sci. Total Environ. 716, 136534.

Yang, S., Liu, X., Cao, H., Guo, B., 1998. Vegetation change on burn blank in Daxing'anling forest area (in Chinese). J. Northeast For. Univ. 26, 19–22.

Yang, Z., Zhou, G., Yin, X., Jia, B., 2014. Geographic distribution of Larix gmelinii natural forest in China and its climatic suitability (in Chinese). Chin. J. Appl. Ecol. 33, 1429–1436.

Zhai, M., Yi, W., Ja, L., Ma, L., Sun, Y., Liu, Z., Wang, Y., 1990. Investigation and study on mixed forest of Hingan larch and white birch in Xilinji (in Chinese). Northeast. For. Univ. 12, 78–85.

Zhang, Q.L., He, H.S., Liang, Y., Hawbaker, T.J., Henne, P.D., Liu, J.X., Huang, S., Wu, Z. W., Huang, C., 2018a. Integrating forest inventory data and MODIS data to map species-level biomass in Chinese boreal forests. Can. J. For. Res. 48, 1–19.

Zhang, Q.L., Liang, Y., He, H.S., 2018b. Tree-lists estimation for Chinese boreal forests by integrating Weibull diameter distributions with MODIS-based forest attributes from kNN imputation. Forests 9.

Zhou, Y., 1991. Vegetation in Great Xing'an Mountains of China. Science Press, Beijing (in Chinese).

Zhu, J.J., Kang, H.Z., Tan, H., Xu, M.L., 2006. Effects of drought stresses induced by polyethylene glycol on germination of Pinus sylvestris var. mongolica seeds from natural and plantation forests on sandy land. J. For. Res. 11, 319–328.

Zhu, Z., Woodcock, C.E., 2012. Object-based cloud and cloud shadow detection in Landsat imagery. Remote Sens. Environ. 118, 83–94.